Construction and Building Materials 443 (2024) 137628

Contents lists available at ScienceDirect

Construction and Building Materials

journal homepage: www.elsevier.com/locate/conbuildmat

Flexural performance of glulam timber beams with glued-in BFRP rods connections

Yaser Jemaa, David Yeboah, Michaela Gkantou *

School of Civil Engineering and Built Environment, Liverpool John Moores University, UK

ARTICLE INFO

Keywords:
Glulam timber beams, BFRP, four-point bending, glued-in rods
Capacity
Rotational stiffness

ABSTRACT

Glued-in rods technique (GiR) is an attractive, yet a relatively new, option to effectively connect structural timber members. With timber buildings accounting for almost 90 % of single-storey residential buildings in developed countries, this technique could be an effective answer for the rehabilitation of aging existing timber beams, thus serving to enhance sustainability and circularity in timber construction. Compared to steel rods, the use of fibre reinforced polymer (FRP) rods could provide additional benefits due to lower weight, better corrosion resistance and lower thermal conductivity. Research on the behaviour of members bonded with Basalt FRP glued-in rods is limited. Nevertheless, until now, there is still no guidance for fabrication and design of such members with any type of FRP rods. The present paper reports an experimental programme on the ultimate performance of glued laminated (glulam) timber beams bonded with glued-in BFRP rods. The article's research significance lies in the type, rod arrangement and material of the glued-in rods connection. In particular, the article examines experimentally four connection types, with the key studied parameters being the rod diameter (8 mm and 10 mm) and the rod arrangement (D1: two rows of 2 rods each over the cross-section, one row on the tensile zone and one row on the compression zone; D2: four rods aligned vertically across the beam's depth). Four replicates were tested for each connection type, leading to a total of 16 test specimens. A four-point bending arrangement with a 2300 mm span was adopted to determine the moment capacity of the connections. Load-displacement response and failure mechanisms were monitored and evaluated. The prominent failure mode observed was bar pull-out and tensile splitting of timber. Design D1 connections with 10 mm bars exhibited the best performance in terms of moment capacity and maximum displacement at failure. The article also offers insights into the observed strain and FRP-adhesive-timber bond behaviour of GiR rods via the use of strain gauges attached to the embedded rods. Addressing the absence of design guidance for such members, the paper proposes theoretical models capable of predicting their moment capacity and the rotational stiffness. In particular, the proposed models achieved mean values of 1.15 for the moment resistance and of 0.99 for the rotational stiffness compared to the experimental data.

1. Introduction

The recent issues of climate change, particularly the rapid increase of carbon dioxide emissions, have contributed towards a growing global shift towards highly sustainable construction materials such as timber. Engineered timber-framed structures can achieve similar strength and stability but with lower embodied energy than their concrete-framed counterparts [1]. Yet, the fast depletion of forests and variability of natural timber samples means it is always difficult to reproduce reliable timber members in larger quantities. Timber beam leftover and other types of timber cuts, which in most cases are considered waste, can be made into new timber elements using timber connections with glued-in rods (GiR). This could serve as a possible remedy to the lower production volume and in turn serve to enhance sustainability and circularity in timber construction. This technique could also be an effective answer to the issue of rehabilitating existing timber structures. Currently, the rehabilitation of such structures holds a great social importance and a significant impact on the economy in most of the European Union countries [2]. For example, timber buildings account for almost 90 % of single-storey residential buildings in developed countries [3,4] and up until now, all adopted intervention methods would avoid recovery and instead opt for completely replacing the aging or damaged timber with

* Corresponding author.
E-mail address: m.gkantou@ljmu.ac.uk (M. Gkantou).

https://doi.org/10.1016/j.conbuildmat.2024.137628
Received 15 March 2024; Received in revised form 9 July 2024; Accepted 24 July 2024
Available online 11 August 2024

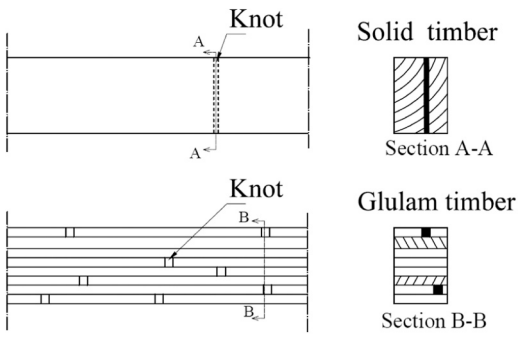

Fig. 1. Defects and natural imperfections dispersed in timber (adapted from [13]).

Table 1
Typical mechanical properties of FRP materials [17]; [22].

Material	Density (kg/m^3)	Tensile strength (MPa)	Yield strength (MPa)	Elastic Modulus (GPa)
Steel	7800	400 – 700	275 – 500	200
AFRP	1450	3000	-	77–135
CFRP	1500	1600	-	200–300
BFRP	2700	1000	-	90
GFRP	1800	850	-	46

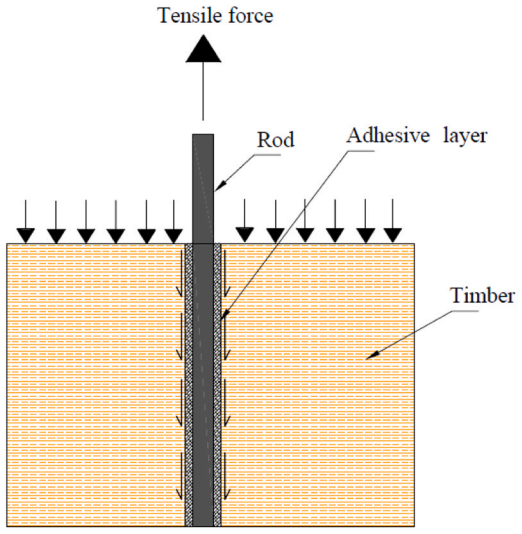

Fig. 2. Load transfer in GiR technique (adapted from [32]).

similar cross-section elements [2].

Conventional timber connections, such as nailed or bolted connections, require longer machining times, excessive labour and yet are only suitable for smaller loads. Conversely, GiR connections [5] offer higher strength, stiffness and fire resistance, in addition to being practically more ductile [6] and lower in terms of production and material costs [7]. Other advantages of glued-in rods are improved aesthetics and fire resistance (because the rods are completely embedded in the host timber). The glued-in rod technique has been used for strengthening of timber perpendicular to the grain, using steel rods as connectors in the jointing system. However, in some studies, steel rods were found to result in splitting failures due to wedging and prying actions [8], whereas in other studies steel rods coated with zinc showed signs of corrosion [9]. The use of fibre reinforced polymer (FRP) rods, as an alternative to steel, results in connections with improved durability, resistance to corrosion, better compatibility with adhesives; and a lower self-weight [10,11]. This makes them ideal for constructing new timber structures with large spans or larger sections as well as strengthening existing ones. A prime example of their use is the Eastview Baptist Church in Auckland which was built in 2003 and the space trusses in Spain constructed out of hollow glued-laminated timber elements with GiR connections. While the production process usually requires strict quality control making them difficult to manufacture on site [12], for smaller sections, however, such as timber beams in residential homes or floor joists, where the required embedment length is relatively small and large holes are provided, the process becomes easy and achievable on site. This is demonstrated in this research in Section 3.

1.1. Research significance

Until now, majority of research on the GiR technique has focused on Glass FRP (GFRP) rods. Research on other FRP variants such as Basalt FRP (BFRP), which offer relatively equivalent or even superior performance to GFRP considering the price, are very limited. Moreover, despite the clear advantages of the GiR over other conventional joint techniques, its application in design is currently rather limited due to lack of reliable design standards [12]. To address these knowledge gaps, the present research investigates the performance of timber beam-to-beam joints with BFRP rods. Unlike natural timber, glued laminated (glulam) members have several advantages, as glulam panel products can be arranged so that the dimensions become independent of the tree species, making the product dimensionally stable [13]. Hence, glulam timber samples are investigated herein. Variables considered in the current research were the effect of the design types and of the rod diameter on the capacity and behaviour of the glulam samples. In addition, the article also offers insights into the observed strain distribution at the FRP-adhesive interface via the use of strain gauges attached to the embedded BFRP rods, which was mainly covered numerically in past studies [14], due to the difficulty associated with the

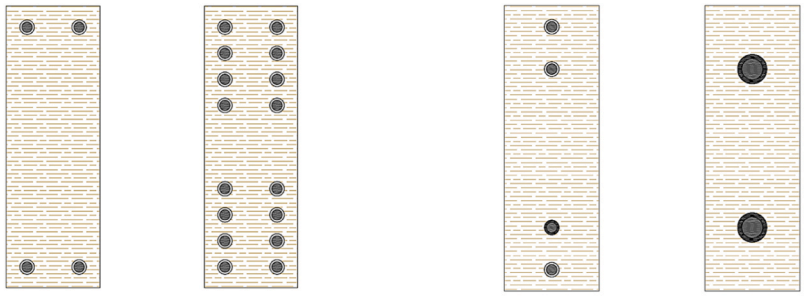

(a) adapted from Xu et al. (2012) *(b) adapted from Madhoushi and Ansell (2008)*

Fig. 3. Schematic illustrations of cross-sectional configurations of glued-in beams.

Table 2
List of timber specimens.

Reinforcement Type	Hole Diameter (mm)	Bar Diameter (mm)	Adhesive Thickness (mm)	Bonded Length (mm)	Configuration	Replicates	Designation
BFRP	14	8	3	160	D1	4	8 - D1–1 8 - D1–2 8 - D1–3 8 - D1–4
BFRP	14	8	3	160	D2	4	8 - D2–1 8 - D2–2 8 - D2–3 8 - D2–4
BFRP	14	10	2	200	D1	4	10 - D1–1 10 - D1–2 10 - D1–3 10 - D1–4
BFRP	14	10	2	200	D2	4	10 - D2–1 10 - D2–2 10 - D2–3 10 - D2–4

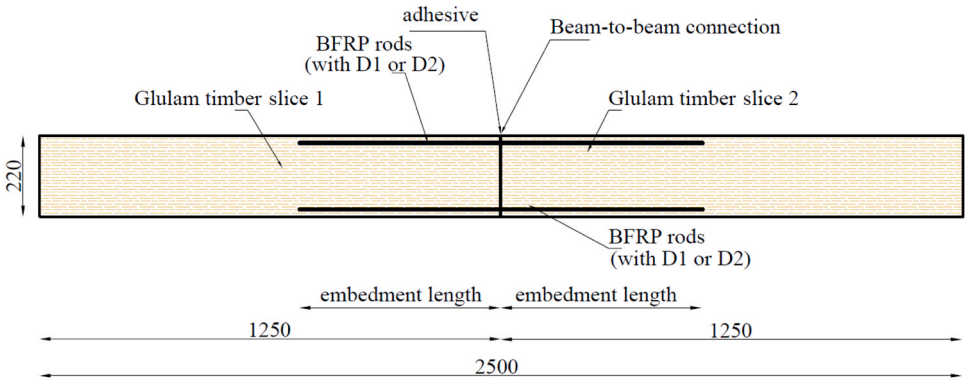

(a) Bonded specimen (from slices 1 and 2)

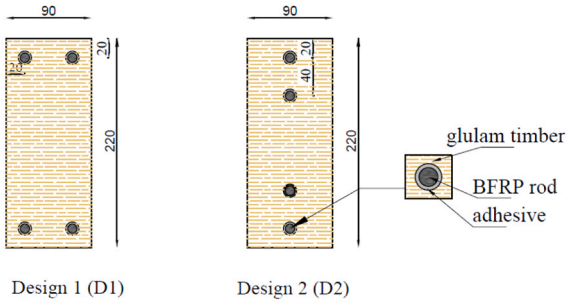

(b) Cross section – design configurations (D1 and D2)

Fig. 4. Bonded specimens with GiR connections (dimensions in mm).

fixing of strain gauges along the embedment length of the rods. Upon discussing background and past research in the field in Section 2, the experimental programme performed is presented in Section 3. The results, including evaluation of failure loads and patterns, are reported in Section 4. Based on the test results, a theoretical model able to predict the performance of the bonded members is presented in Section 5. The results provide a sound basis for developing guidelines for the design of the structural timber connections with GiR.

2. Background and previous research

The present section provides background and previous research on topics relevant to the experimental programme conducted herein. Materials used for fabricating GiR connections are the host timber, the adhesive and the connecting rod. The constituent materials, i.e., glulam timber (Section 2.1), FRP rods (Section 2.2), and the timber-FRP structures (Section 2.3) are initially presented. Following, adhesives for GiR (Section 2.4), connections configurations (Section 2.5), theories (Section 2.6), failure mechanisms (Section 2.7) and beam tests (Section 2.8) of the GiR technique are discussed.

2.1. Glulam timber

Glulam timber members are manufactured by joining layers of sawn timber with resins [15]. The use of glulam members results in higher capacity (strength and stiffness) because natural imperfections, such as

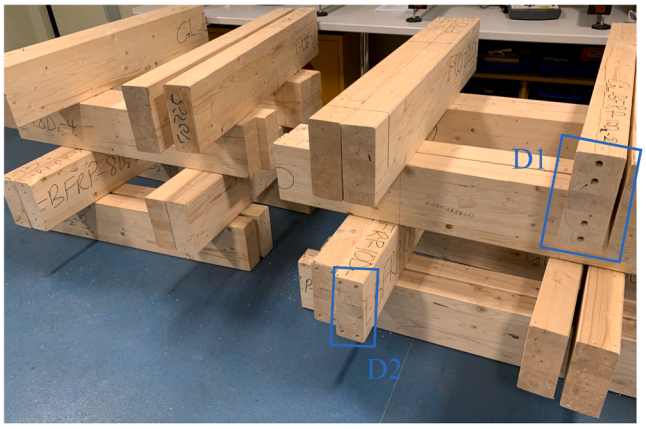

(a) Glulam slices in pairs – holes drilled for the two configurations (D1, D2)

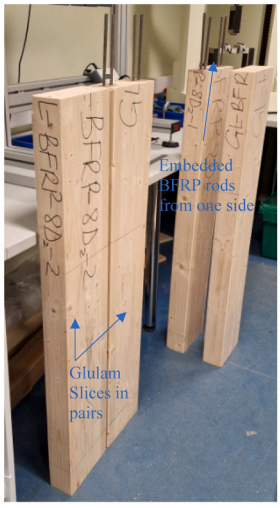

(b) Glulam slices in pairs - epoxy adhesive inserted in the holes of one glulam slice - BFRP rods embedded

Fig. 5. Fabrication of beam-to-beam connections.

juvenal wood, knots and cross grains are more consistently dispersed throughout the cross-section (see Fig. 1), which thus becomes dimensionally stable [13].

2.2. Fibre reinforced polymer (FRP)

FRPs are load bearing composite materials that appear enhanced load transfer between the fibres. There are several types of FRPs used in construction and their application depend on factors such as fibre material, orientation, and fraction. The most common FRPs are glass (GFRP), carbon (CFRP), aramid (AFRP), and basalt (BFRP), whose main mechanical properties are listed for reference in Table 1. As can be seen, FRPs have lower elastic modulus compared to steel and hence could be better compatible with timber structures. Moreover, they have higher tensile capacities, which means that less amount will be required [16-21]. Several studies have shown the potential of BFRP rods as replacement of steel rods in the construction industry and hence BFRPs will be investigated in this study.

2.3. Timber-FRP applications

Application of FRPs for strengthening of timber structures began in the mid-1960s and is becoming increasingly popular. Various types of FRP reinforcement (strips, sheets, rods) can be applied to effectively restore the load-bearing capacity of damaged elements with minimal interference to the aesthetics of the structure [23]. Examples of recent research studies include the experimental study by Wu et al. [24] on the use of GFRP plate for connecting timber elements, the work by Kilinçarslan et al. [25] examining the behaviour of beams, reinforced with carbon CFRP composites in a "U" shape at the bottom layer and the experimental work by Corradi et al. [26] who suggested locally applied FRP sheets in the area where defects were noted. Due to lack of design standards for FRP-strengthened timber structures, there is also ongoing research on theoretical models, such as the proposal of [27] on modelling of timber beams strengthened with FRPs. Another important research topic regards the non-destructive evaluation of FRP-timber interface condition [4]. Additional studies of FRP-timber applications have proposed using FRP tendons for prestressing timber members and using FRPs for glued-in rod technique [28,29]. Zhang et al. [12] recently presented a review on glued-in rods (GiR) connections, their main influencing factors, failure mechanisms and their design methods. GiR technique is the focus of the present research.

2.4. Adhesives for GiR

In glued-in rod technique (GiR), adhesives play a critical role for achieving good adhesion of the rod to the timber, particularly in cases of rods with smooth outer surfaces [21,30]. The adhesive carries the load transfer between the timber and the reinforcement or connecting rods (see Fig. 2), thus the performance of the connection depends on the shear capacity of the employed adhesive. Factors such as ease of application, consistency with the host timber and the FRP, and curing time are important in the selection of adhesives for bonding [10]. Several adhesives have been applied in connection with glued-in rod technique. Traditional adhesives, such as phenolphthalein-resorcinol (PRF), polyurethanes (PUR) and epoxies (EPX) have been reported [30]. The selection of the adhesive for bonding of FRP to timber has to be undertaken with great care [31].

In GiR technique, the adhesive should have gap-filling properties for optimum performance. Whilst several adhesive types have been shown to provide satisfactory bonding in a controlled environment, two-part cold-cure epoxy adhesives have generally been found to be most suitable for on-site bonding. Harvey and Ansell [10] investigated the behaviour of glued-in rod connections with GFRP bars bonded with epoxy adhesives. They tested samples with different glueline thickness ranging from 0.5 mm – 6 mm. They reported that a glueline thickness of at least 2 mm gives ultimate results for epoxy adhesives. Madhoushi and Ansell [14] used finite element analysis to investigate the effect of glueline thickness (0.5 mm, 1 mm, 2 mm and 4 mm) on the behaviour of glued-in rods. An increase of the thickness resulted in a decrease in the stress concentration in the Z-direction across the glueline thickness from the rod-adhesive interface towards adhesive-timber interface of the specimens. Epoxy adhesives have been successfully used for strengthening and repair of timber samples in GiR, achieving good ultimate capacity results [33,7,34]. These will also be applied in the experimental study presented in Section 3.

2.5. Configuration of GiR FRP timber connections

For the fabrication of the GiR connections, oversized holes are drilled or machined through the timber, in accordance with predetermined bonded length and providing respective gap of 1–2 mm between the host timber and the rod. Steiger et al. [7] have concluded that small glueline thickness are preferable, since most of the adhesives perform better in thinner adhesives, whilst Harvey and Ansell [10] have recommended that the glueline thickness that resulted in maximum bond strength was at least 2 mm. Harte and Dietsch [17] suggested that during fabrication, the fibres of FRP members should be parallel to load, as the FRPs are strong in direction parallel to the fibres. Typical configuration of beam-to-beam connections using glulam samples are shown for reference in Fig. 3 [35].

(a) photo of the set-up

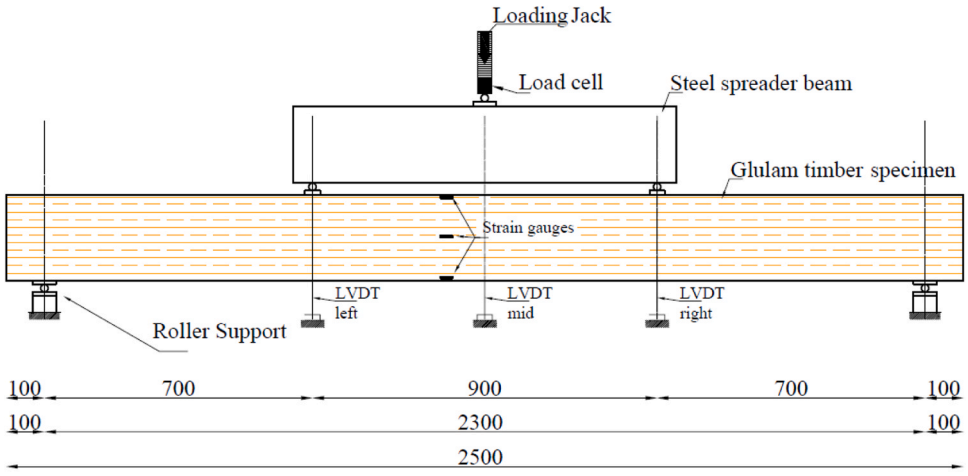

(b) schematic illustration of the set-up

Fig. 6. Four-point bending test set-up.

Table 3
Evaluation of initial global bending of the specimens and rotational stiffness of the connection.

Specimen	Bending Stiffness EI (Nmm^2)	Rotational Stiffness k (kNm/rad)
8 - D1–1	6.38E+11	1264
8 - D1–2	5.95E+11	1184
8 - D1–3	4.65E+11	883
8 - D1–4	5.11E+11	993
mean	5.97E+11	1081
8 - D2–1	3.89E+11	788
8 - D2–2	6.82E+11	1184
8 - D2–3	7.10E+11	1408
8 - D2–4	6.15E+11	796
mean	6.71E+11	1044
10 - D1–1	5.64E+11	1220
10 - D1–2	6.31E+11	1251
10 - D1–3	6.08E+11	1254
10 - D1–4	7.39E+11	1414
mean	6.60E+11	1285
10 - D2–1	5.31E+11	1066
10 - D2–2	6.26E+11	1215
10 - D2–3	6.01E+11	1202
10 - D2–4	6.78E+11	1328
mean	6.40E+11	1203
Mean (ALL)	6.30E+11	1153
COV (ALL)	6 %	17 %

2.6. Behaviour of GiR connections

Several factors can affect the behaviour and capacity of connections with GiR. Pull-out tests are normally conducted to investigate factors affecting the GiR connections, to describe their behaviour and to give the basis for the design of moment connections. Some of the factors that affect the bond performance of the connections are the host timber, the type of connecting rod, the type of adhesive, the bonded length, the rod diameter, the glueline thickness and the edge distance [10,34,21]. Steiger et al. [7] stated that the bond between the rod and the resin behaves as a mechanical joint, which depends on factors such as adhesive strength, characteristics of the surface of the rod and surface treatment of the connecting rod. Zhu et al. [21] suggested that the capacity of the connections with GiR FRP depends on the surface area of the rods as well as the shear strength of the interfacial adhesive/timber zone. Hence, it has been recommended that adhesives, such as epoxy with better gap-filling properties should be employed for the fabrication, whilst for strong bond, the FRP should be sanded or abraded and glued in freshly machined or drilled timber samples.

The relationship between the bond capacity and the factors of geometry (bonded length, rod diameter, hole diameter) is complex, since the type and behaviour of the adhesives highly influence the pull-out capacity. It has been shown that an increase in bonded length and rod diameter generally resulted in corresponding increase in bond capacity of the connections [7,36]. Buchanan et al. [8] showed that ultimate

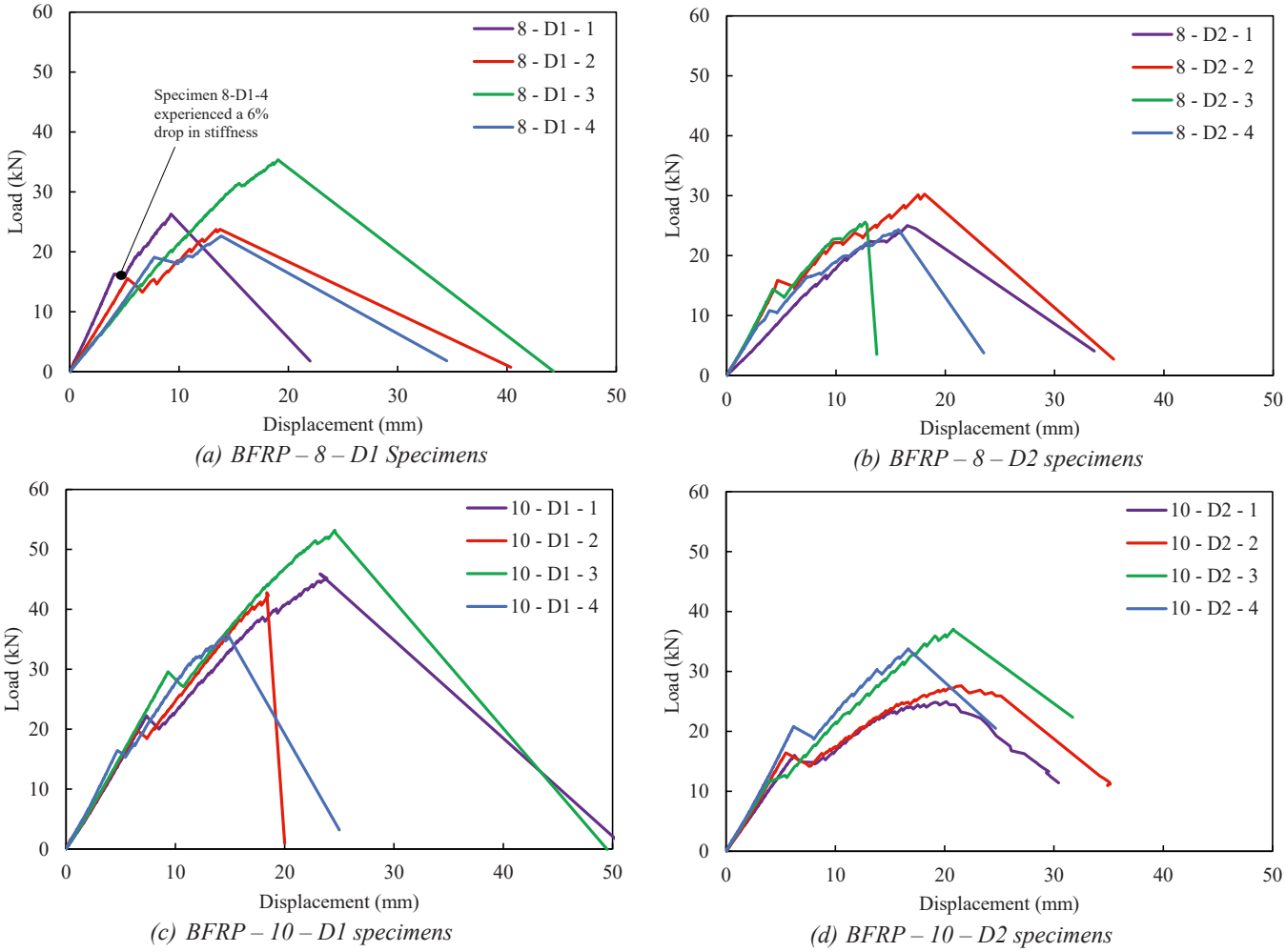

Fig. 7. Load- midspan displacement curves for all specimens.

Table 4
Failure load ($N_{u,Exp}$), moment resistance ($M_{u,Exp}$), corresponding mid-span displacements ($\delta_{u,Exp}$).

Specimen	$N_{u,Exp}$ (kN)	$M_{u,Exp}$ (kNm)	$\delta_{u,Exp}$ (mm)
8 - D1–1	26.30	9.21	12.69
8 - D1–2	23.76	8.32	13.74
8 - D1–3	35.37	12.38	19.30
8 - D1–4	22.64	7.92	13.85
8 - D2–1	25.02	8.76	16.53
8 - D2–2	30.26	10.59	18.10
8 - D2–3	25.58	8.95	12.65
8 - D2–4	24.35	8.52	15.72
10 - D1–1	45.91	16.07	23.23
10 - D1–2	42.78	14.97	18.36
10 - D1–3	53.20	18.62	24.58
10 - D1–4	35.33	12.37	14.88
10 - D2–1	24.96	8.74	20.14
10 - D2–2	27.62	9.67	21.53
10 - D2–3	37.07	12.97	20.79
10 - D2–4	33.80	11.83	16.68

performance for GiR GFRP connections was found for bonded length equal to 15×hole diameter or 20×rod diameter. GIROD [30] recommended a minimum bonded length of 0.4×rod diameter^2 or 8×rod diameter. In addition, it has been recommended that the edge distance should be at least 2.5×rod diameter to prevent pre-mature splitting. Harte and Dietsch [17] observed that the ratio of the hole diameter to rod diameter affects the load transfer mechanism of the connection.

Moisture content is another important parameter influencing the behaviour of the connections [37]. Experiments by [38] showed that an increase in moisture content by 1 % resulted in 2.5 % decrease in shear strength of the timber sample. GIROD [30] developed a calculation model of glued-in rods. The moisture content for the test samples was 12 % or less at room temperature of 20°C and 65 % relative humidity. Harvey and Ansell [10] observed that cracks can occur at the end of the rods, if the moisture content of the timber samples is above the equilibrium moisture content of the surroundings. The effect of timber density on the joint strength of GiR specimens was examined by Chans et al. [36], who observed that the average shear capacity of the samples increased with increase in density.

2.7. Failure mechanisms of GiR connections

The glued-in rod connections behave as a chain made up of series of links of rod, adhesive and timber. Possible failure mechanisms for GiR samples are failure of the rod in tension or compression, shear failure of timber or wood close to the bond line, failure of the adhesive and timber splitting [30,39]. The most important failure mode is the shear failure/fracture of timber close to the interfacial timber/adhesive zone [39,40]. The adhesive failure at the interfacial timber/adhesive zone or the fracture of wood close to the glueline due to cohesive force can lead to bar pull-out. Gardelle and Morlier [39] suggested that the shear capacity of the adhesive should be higher than the timber in order to provoke failure to occur in the timber, which is the weakest link of the connection. Tensile splitting failure occurs in timber mainly due to inadequate

Table 5
Failure mode and observations at failure.

Specimen	Failure mode
8 - D1–1	• Splitting of timber along the bar at tension and compression zone • Pull-out of bars at tension zone
8 - D1–2	• Splitting of timber along the bar at tension zone • Pull-out of bars at tension zone • Splitting of timber at compression zone
8 - D1–3	• Pull-out of bars at tension zone • Splitting of timber along the bar at compression zone • Splitting of timber along the bar at tension zone with wood attached to the bonded bars
8 - D1–4	• Pull-out of bars at tension zone • Splitting of timber along the bar at tension zone
8 - D2–1	• Splitting of timber along the bar at compression zone • Interface timber and glue debonding • Pull-out of bars at tension zone with wood attached to the bonded bars
8 - D2–2	• Pull-out of bars at tension zone • Interface timber and glue debonding • Splitting of timber along the bar at tension zone
8 - D2–3	• Pull-out of bars at tension zone • No splitting
8 - D2–4	• Pull-out of bars at tension zone • Slight splitting at the soffit of the beam
10 - D1–1	• No pull-out of the bar • Tensile failure along the bar at compression zone • Grain failure • Splitting of timber at tension and compression zone
10 - D1–2	• Pull-out of bars at tension zone with wood attached to the bonded bars. • Splitting of timber along the bar at tension and compression zone
10 - D1–3	• Debonding • Splitting of timber along the bar at compression zone • Splitting of timber at tension zone at soffit and size of beam
10 - D1–4	• Debonding of epoxy glue • Pull-out of bars at tension zone with wood attached to the bonded bars. • Splitting of timber at compression zone
10 - D2–1	• Splitting of timber along the bar at tension and compression zone • Pull-out of bars at tension zone
10 - D2–2	• Pull-out of bars at tension zone • Slight splitting at the compression zone
10 - D2–3	• Debonding at the timber/adhesive interface • Pull-out of bars at tension zone • Splitting at the soffit of the beam • Splitting of timber at compression zone
10 - D2–4	• Debonding at the timber/adhesive interface • Pull-out of bars at tension zone • Splitting of timber at compression zone • Splitting of timber around knot at compression zone

edge distance or rod-to-rod distance. It can also occur when the rod is not inserted perfectly parallel to the grain of the timber specimen or when the samples are loaded excessively perpendicular to the grain [30].

2.8. Capacity and design of GiR FRP connections

Past research on GiR connections with FRP rods has mostly focused on tensile pull-out of specimens (mostly single rod) and the influence of key parameters, whereas research on the capacity and design of the connections has been relatively limited. In addition, most investigations are on carbon and glass FRP rods, while research on GiR BFRPs connections are scarce.

Harvey and Ansell [10] investigated the performance of spliced beams (with inline joints) and T-piece joints using GFRP rods bonded in LVL timber with epoxy adhesives. The spliced beams were tested under four-point loading, whilst the T-piece joints were subjected to tension induced bending moment and lateral shear force. The inline or spliced beams failed by splitting of timber along the grain. The researchers recorded ductile behaviour in some of the T-piece samples. Three glulam joint specimens made using beams connected with CFRP rods glued by

(a) 10 – D1 – 3: Debonding; Splitting of timber along the bar at compression zone; Splitting of timber at tension zone at soffit and size of beam

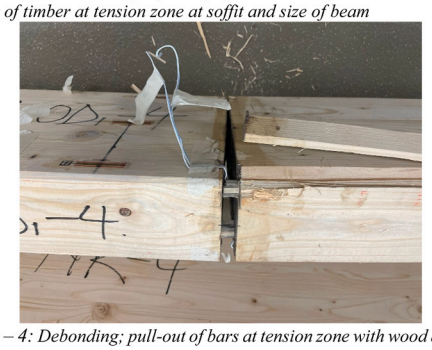

(b) 10 – D1 – 4: Debonding; pull-out of bars at tension zone with wood attached; splitting of timber at compression zone

(c) 10 – D2 – 3: Debonding at the interface; pull-out of bars at tension zone; splitting at the soffit of the beam; splitting of timber at compression zone

(d) 8 – D2 – 2: Pull-out of bars at tension zone; Interface timber and glue debonding; splitting of timber along the bar at tension zone

Fig. 8. Typical failure modes.

epoxy resin were investigated by [29]. [41,42] studied experimentally the performance on beam-to-beam and beam-to-column connections with glued-in GFRP rods under static and fatigue loading. By comparing the test results of the beam-to-beam connections with solid beams, it was found that the latter can achieve higher load capacity but they allow for lower dissipated energy. The use of BFRP as connecting rods for GiR in moment resisting structures has been investigated by O'Neill et al. [43]. The diameter of the rod used was 12 mm. A 2-component epoxy adhesive, with good gap-filling properties, with glueline thickness of 2 mm was used. The experimental programme also comprised testing of portal frames, which were fabricated with different configurations with respect to the number of BFRP rods (2 and 3 rods) and the web materials. The

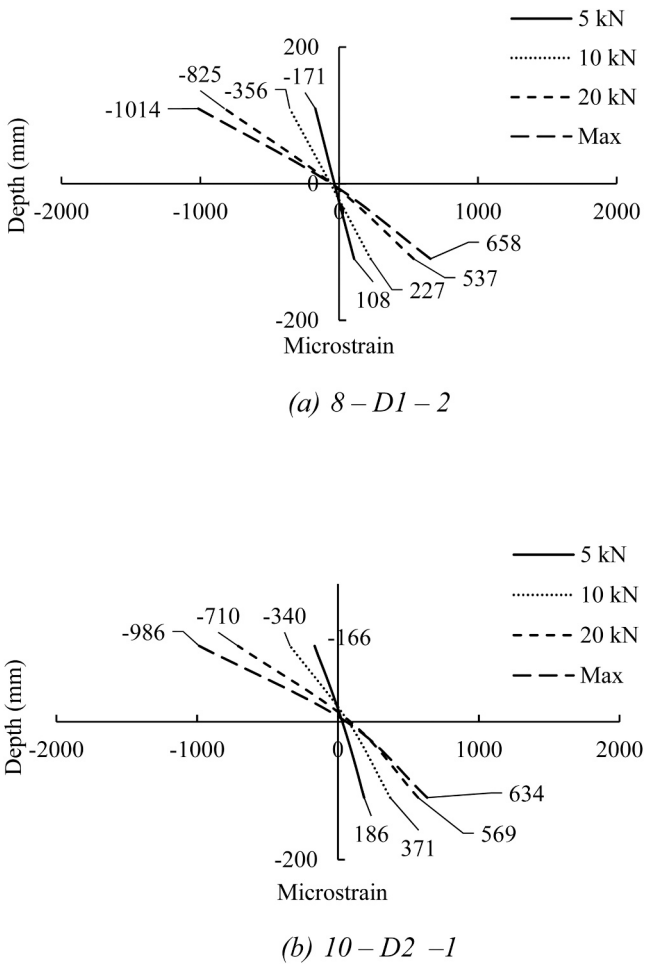

Fig. 9. Typical load-strain curves for D1 and D2 specimens.

experimental research showed that an increase in BFRP rods (3 rods) did not significantly increase the overall capacity of the moment-resisting frame corner. However, the variability within the samples increased by around six times when another rod was added.

Given the limited research data on GiR connections with FRP rods and the difficulty in understanding the behaviour of these connections, there is still no standard guidance for the fabrication and design rules in place due to difficulty in understanding the behaviour of the connection. [44] has proposed basic guidelines in the design of GiR which are enshrined at the Annex A. To address these gaps and obtain a better understanding on GiR connections with FRP rods, an experimental programme is presented hereafter.

3. Experimental programme

3.1. Materials

The timber beams used for the experiment were made of glued laminated timber of grade GL28h with characteristic bending strength of 28 MPa and had a nominal cross-section of 90 mm × 220 mm. The thickness of each lamination of the glulam was 44 mm. The BFRP rods used were supplied by [45] from their RockBar range. They have an elastic modulus of 54 GPa and a tensile strength of 920 MPa [46]. Two BFRP rod diameters were employed, namely 8 mm and 10 mm. Two-part epoxy adhesives, which are known to have good gap-filling, shrinkage and thixotropic properties, were adopted. They were supplied by [47] and have a nominal shear strength of 12.5 MPa [48].

3.2. Fabrication of bonded timber specimens

A total of 16 bonded specimens were tested within this study. The specimens can be categorised into four groups, each containing four replicates, as listed in Table 2. All specimens included a beam-to-beam connection at midspan. The connection consisted of BFRP rods embedded through a length of 20×bar diameter on either side and glued in with epoxy-adhesive of 2–3 mm epoxy thickness, for 8 mm and 10 mm bars, respectively, as depicted in Fig. 4. BFRP rods were embedded in two different design configurations (D1 and D2), according to Fig. 4, and in two diameters, i.e., 8 mm and 10 mm. Both configurations included two bars on the tension and two on the compression zone, but in D1 the bars were placed in the same horizontal line, whilst in D2 all four bars were in a vertical line (see Fig. 4b). The designation applied in Table 2 shows the rod diameter, the design configuration and the replicate number.

The fabrication procedure of the bonded beam specimens is shown in

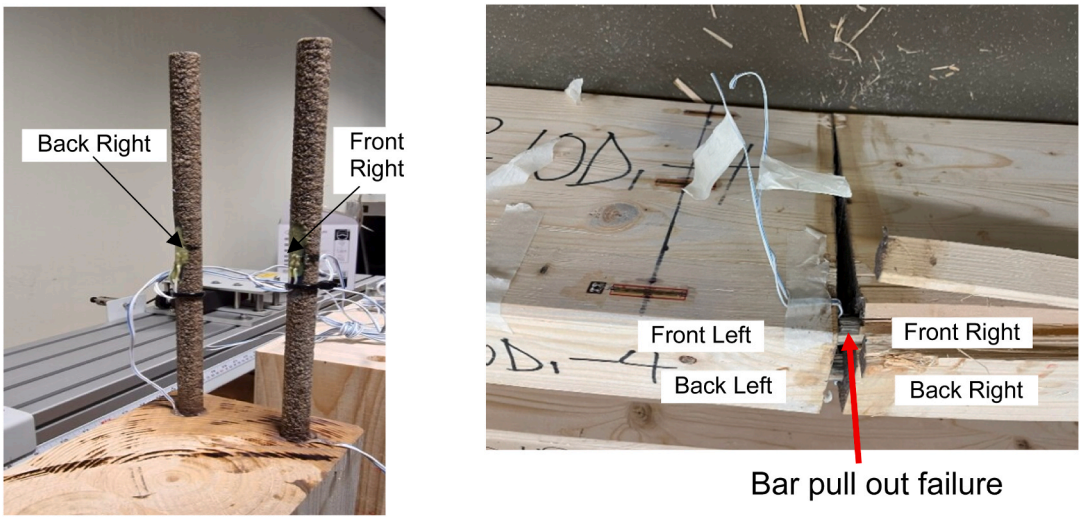

(a) Strain gauges on FRP bars during fabrication process

(b) Photo at failure and demonstration of strain gauges' locations

Fig. 10. Bar pull-out failure observed on the right-hand side of specimen (10 – D1 – 4).

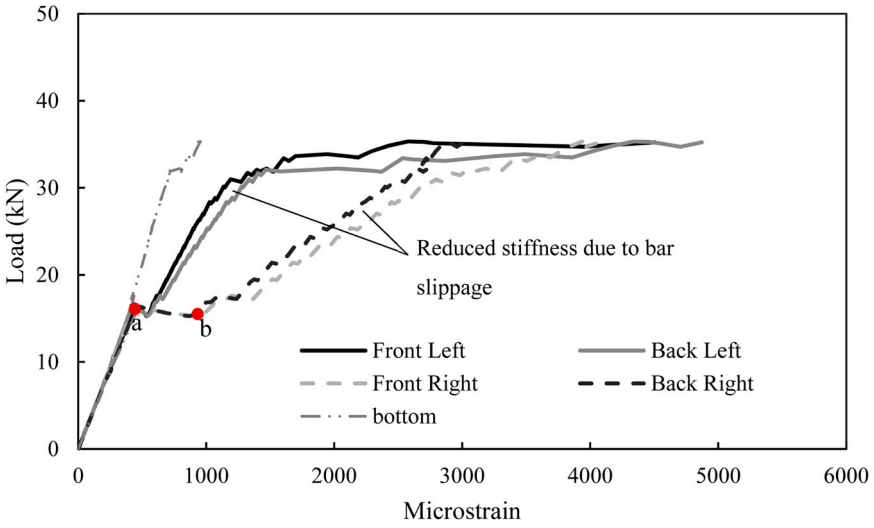

Fig. 11. Measurements of the strain gauges attached on bars (10 – D1 – 4).

Fig. 5. Two 1250 mm long slices were used for the fabrication of each specimen. Two 10 mm thick steel plates with pre-drilled holes, one for each design configuration, were manufactured to guide the drilling bit and consistently achieve accurate results. Holes were drilled on one side of each slice, as per the two design configurations of Fig. 4(b). The vertical distance between the centre of the rod to the timber's edge is 20 mm for both designs. All holes had a 14 mm diameter allowing for 2 mm and 3 mm glueline thicknesses for the 10 mm and 8 mm rods, respectively [10]. According to Buchanan et al. [8] and Bengtsson and Johansson [30], the adopted embedment length was $20d_r$ where d_r the rod diameter, making it 160 mm for specimens with 8 mm rods and 200 mm for the joints with 10 mm rods, as shown in Fig. 4.

Once drilling was complete, holes were thoroughly cleaned using a cylinder metal brush and pressurised air. The base and the hardener of the epoxy were thoroughly mixed with a mix ratio 1:0.4 for at least 3 minutes, until the material became smooth in consistency and uniform in colour. The epoxy adhesive was then applied to one slice in each pair. To achieve uniform coverage and avoid air pockets, the applicator nozzle was inserted till the end of the pre-drilled hole and then pulled out gradually as the epoxy was being applied. The holes were 2/3 filled, then the BFRP rods were inserted while being rotated (see Fig. 5(b)). The specimens were left to cure in the vertical position for 24 h. The final specimen was then completed by applying epoxy to the second slice which would then be slipped over the other cured slice. A leveller and several clamping devices were then used to straighten the specimens. All specimens were allowed to cure for a minimum of 7 days to achieve optimum strength before testing.

3.3. Testing

A series of four-point bending tests were carried out to study the flexural performance of timber joints. In Fig. 6, both a schematic illustration and a photo of the set-up are depicted. An I-shaped steel stiffened spreader beam was used for load transfer. In order to avoid local stress concentration and enable better load distribution, steel rollers together with steel bearing plates were used at the support points. Three linear variable displacement transducers (LVDTs) were positioned at the two load points and at mid-span to record vertical displacements. Strain gauges, 30 mm long, were attached to the external faces of each specimen at three locations to monitor the strain distribution profiles (see Fig. 6(b)). A data acquisition system was used to log all required data during testing. The monotonic load was applied via displacement control with a constant rate of 3 mm/min [49].

All specimens were tested first for service loading up to 12 kN (20 % of the estimated failure load). Upon application of the service loading, the specimens were loaded to failure. The connection area was subjected to pure bending, with the aim to assess its resistance. The loading was applied in quasi-static monotonic way until failure. Measurements of the applied load, the vertical displacement and the strains were recorded throughout the whole testing.

4. Results and discussion

4.1. Global bending and rotational stiffness

The data recorded during the initial service load were used in order to evaluate the bending stiffness. Eq. (1) was applied in the linear-elastic stage of each beam in order to evaluate the global flexural stiffness (EI)

$$EI = \frac{\alpha \Delta P}{48 \Delta \delta}\left(3L^2 - 4a^2\right) \quad (1)$$

Where ΔP is the range of the applied load and $\Delta\delta$ the corresponding range of the mid-span vertical displacement, E is the Young's Modulus, I is the second moment of area, L is the span of the beam, equal to 2300 mm herein and α is the distance from the loading point to the support equal to 700 mm for this study.

Using Eq. (1), the global bending stiffness has been evaluated for the timber specimens, based on the initial testing. The rotational stiffness of the connections has been calculated as a ratio of the applied bending moment over the corresponding angle of rotations. The results are presented in Table 3. As can be seen, the bending stiffness has an average value of 6.30E+11 Nmm^2 with a fairly low coefficient of variation (6 %), indicating relatively similar bending stiffness in all four configurations tested. In addition, if one considers that the second moment of area (I) is equal to $bh^3/12$, where b and h are the width and depth of the timber cross-section (equal to 90 mm and 220 mm respectively), then the nominal value of $I=79860000\ mm^4$ and thus the average calculated Young's Modulus of the bonded timber specimens would be equal to $E=EI/I=6.30E+11/79860000= 7893.2\ MPa$. It is noteworthy that on a parallel experimental study examining the flexural performance of glulam specimens, a very similar average value has been found for the Young's Modulus of solid glulam beams of same material and dimensions. This shows that the connection configuration has a small effect on the stiffness of the bonded beam. Similar observations have been made by Micelli et al. [29] and Xu et al. [50]. Largest values for the rotational stiffness values, have been achieved by the configuration D1 with 10 mm bars, for which an average value of 1285 kNm/rad was recorded. The observed variations within each group can be attributed

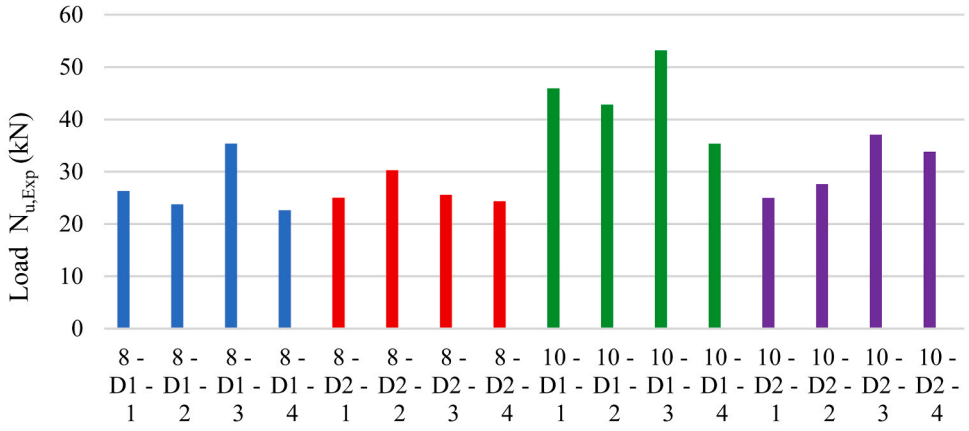

(a) ultimate load ($N_{u,Exp}$)

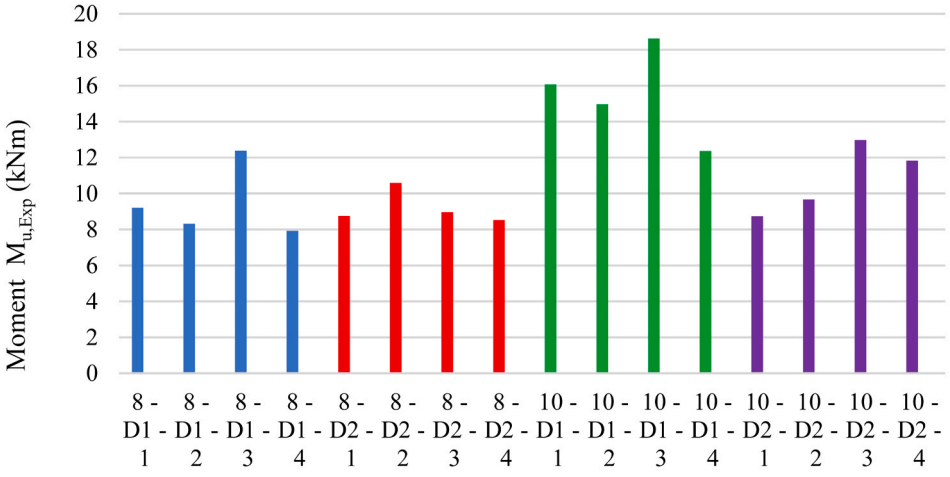

(b) moment resistance ($M_{u,Exp}$)

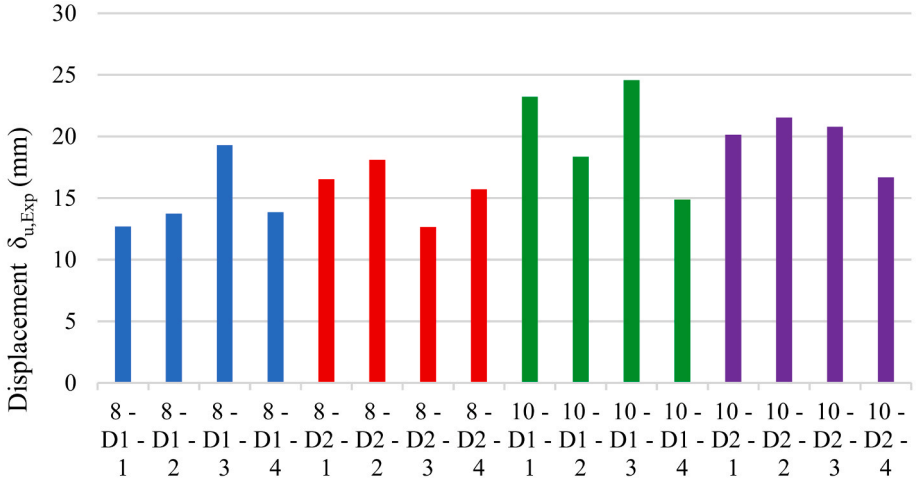

(c) displacement at ultimate load ($\delta_{u,Exp}$)

Fig. 12. Ultimate performance for each examined group.

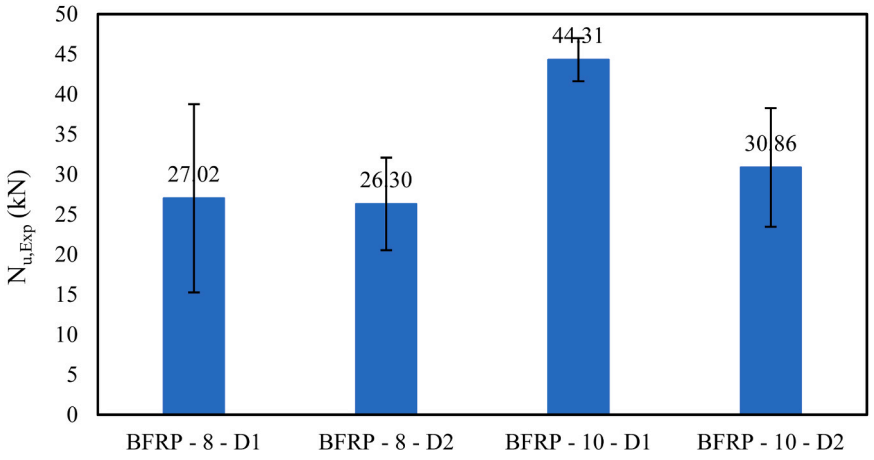

(a) average ultimate load ($N_{u,Exp}$)

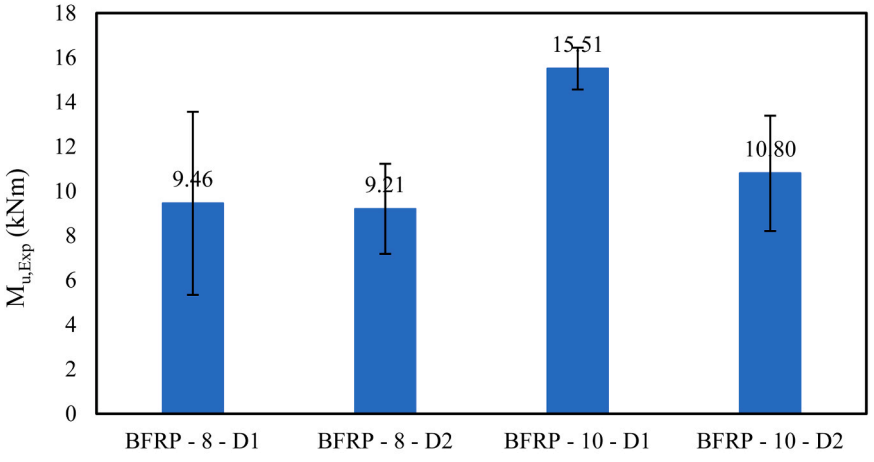

(b) average moment resistance ($M_{u,Exp}$)

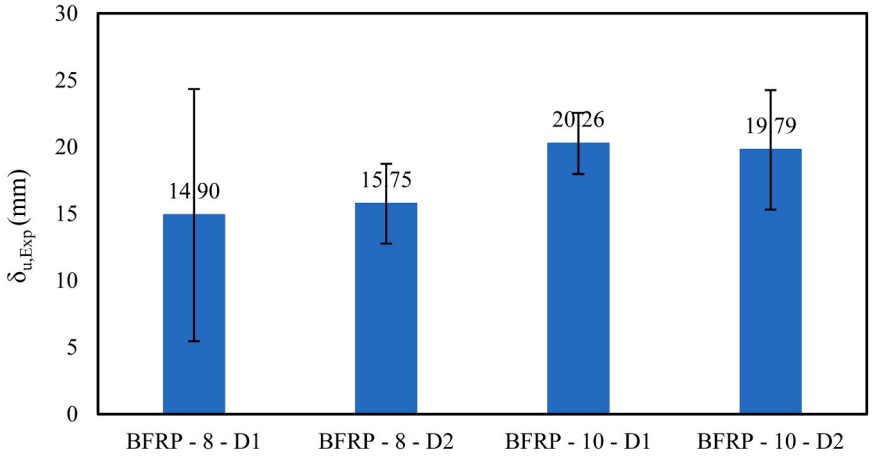

(c) average displacement at ultimate load ($\delta_{u,Exp}$)

Fig. 13. Graphical presentations of average values of ultimate load, moment and displacement.

to factors such as variability within wood species, growth rate, climate conditions and also complexity of interaction and the distribution of defects between the glulam lamellae Similar findings were reported by Sousa et al. [51] and Ekundayo et al. [52].

4.2. Load-vertical displacement curves

The load versus mid-span vertical displacement curves for all tests were recorded and presented in Fig. 7. Each graph presents the response of a group with similar characteristics. In most cases, a small "jump" in

Table 6
Average values of forces, moments and displacements.

Specimen	Replicates	$N_{u,Exp}$ (kN)	$M_{u,Exp}$ (kNm)	$\delta_{u,Exp}$ (mm)
8 – D1	4	27.02	9.46	14.90
8 – D2	4	26.30	9.21	15.75
10 – D1	4	44.31	15.51	20.26
10 – D2	4	30.86	10.80	19.79
8&10 - D1&D2	16	32.12	13.41	17.67

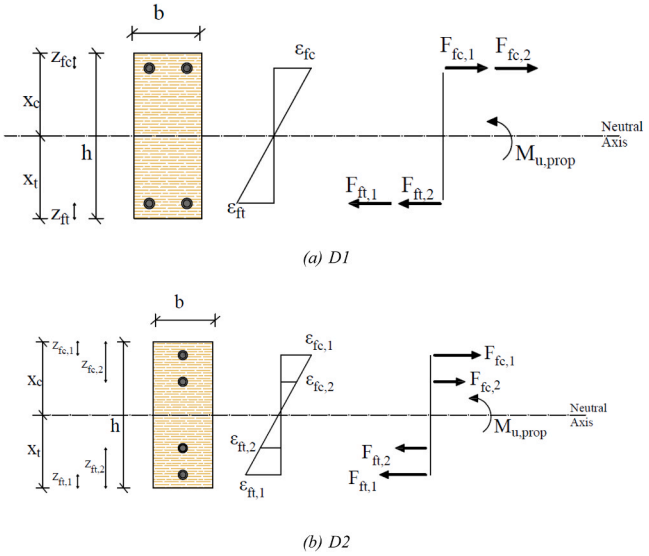

Fig. 14. Model for bending strength prediction.

Table 7
Comparison between proposed and experimental bending strength.

Specimen	$M_{u,Exp}$ (kNm)	$M_{u,prop}$ (kNm)	$M_{u,prop}/M_{u,Exp}$
8 - D1–1	9.21	13.64	1.48
8 - D1–2	8.32	13.64	1.64
8 - D1–3	12.38	13.64	1.10
8 - D1–4	7.92	13.64	1.72
8 - D2–1	8.76	8.73	1.00
8 - D2–2	10.59	8.73	0.82
8 - D2–3	8.95	8.73	0.98
8 - D2–4	8.52	8.73	1.02
10 - D1–1	16.07	17.05	1.06
10 - D1–2	14.97	17.05	1.14
10 - D1–3	18.62	17.05	0.92
10 - D1–4	12.37	17.05	1.38
10 - D2–1	8.74	10.91	1.25
10 - D2–2	9.67	10.91	1.13
10 - D2–3	12.97	10.91	0.84
10 - D2–4	11.83	10.91	0.92
		mean	1.15
		COV	0.24

the load-displacement response, causing a slight change to the initial stiffness, has been observed soon after loading. The jump, which corresponds to the moment a gap opening appeared on the connection interface, is attributed to the breaking of the thin layer of leftover adhesive between the two timber slices. Overall, similar performance between the four replicates of each group has been observed. Further discussions and comparison between the four studied cases are included in Section 4.5.

4.3. Moment resistance and failure modes

During testing, the applied load (N) was incrementally monitored. The maximum recorded value of the load is considered as the failure load ($N_{u,Exp}$) of each specimen. To evaluate the moment resistance, the equation $M_{u,Exp}=(N_{u,Exp}/2)\times\alpha$ where α is the distance from the loading point to the support, was applied. The distance α is equal to 700 mm, for this investigation (see Fig. 6(b)). In Table 4, the failure loads ($N_{u,Exp}$), the moment resistance ($M_{u,Exp}$) and the corresponding mid-span vertical displacements ($\delta_{u,Exp}$) are listed.

In Table 5, the failure modes along with observations during the loading stage are reported. The dominated failure modes were bar pull-out with wood attached and tensile splitting of timber indicating the interface between the adhesive and the FRP rods remained intact. Typical cases are shown in Fig. 8.

4.4. Strain distribution profiles and strain measurements on bars

Fig. 9 shows typical strain distribution profiles of the two design configurations. The development of these graphs was based on the recorded measurements of three strain gauges, see Fig. 6, at four level loads (i.e. 5 kN, 10 kN, 20 kN, Max). These gauges were attached to the beam left side 100 mm from the connection interface at three locations, 25 mm from the top and bottom of the beam to match the location of the embedded bars; and also at mid-height. As expected, bending performance with increasing tensile strains at the bottom part of the beam and compressive strains at the top of the beam have been recorded.

In order to monitor the response of the BFRP bars, strain gauges have also been attached to the bottom bars of specimen BFRP – 10 – D1 – 4, as shown in Fig. 10 (a). A total of four strain gauges have been attached longitudinally to the two bars 100 mm from the connection interface (two at either side of the connection). The overall recorded performance up to point (a) (see Fig. 11) presents increasing tensile strains for increasing load with almost identical stiffnesses observed for all recorded strains. Once the gap opening occurs, indicated by point (a), a significant difference is observed between the different groups of strain gauges. While the external timber strain gauge maintained its initial stiffness, the left and right groups exhibit a reduced stiffness indicating the onset of bar slippage. This bar slippage is especially evident in the continued drop from point (a) to point (b) and the further reduced stiffness for the right group of strain gauges (see Fig. 10 and Fig. 11).

4.5. Discussion

To better visualise the ultimate performance for each examined group of specimens, Fig. 12 presents graphically the ultimate loads, moment resistance and corresponding displacements. The average values for each group of study are also graphically shown in Fig. 13 and Table 6. As can be seen, best performance both in terms of moment resistance and of corresponding displacement, was obtained for the bonded specimens with rods of 10 mm diameter and D1 design configuration. In particular, the joint with 10 mm rods and D1 achieved an average ultimate load of 44.31 kN. As expected, for both D1 and D2, the joints with 10 mm rods outperformed their counterparts with 8 mm rods. In addition, comparing the two proposed designs, enhanced performance has been noted for D1 design for both examined rods diameters (i.e. average $M_{u,Exp}$ equal to 9.46 kNm and 15.51 kNm for 8-D1 and 10-D1, and average $M_{u,Exp}$ equal to 9.21 kNm and 10.80 kNm for 8-D2 and 10-D2).

5. Theoretical analysis

5.1. Bending strength

Theoretical analysis is performed to predict the moment capacity of the in-line bonded beam-to-beam specimens. Assuming a general section

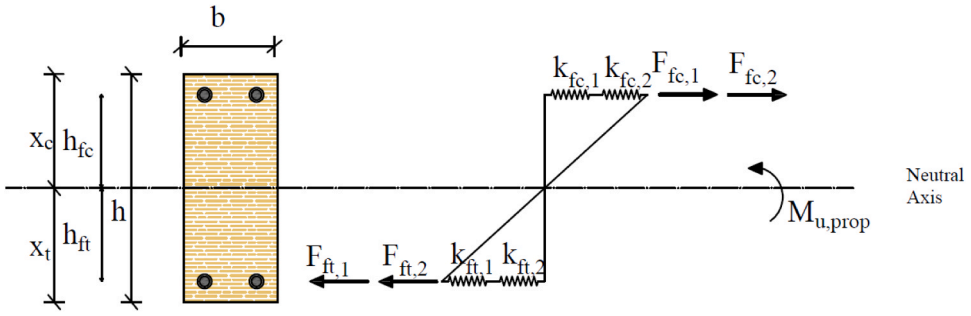

(a) D1

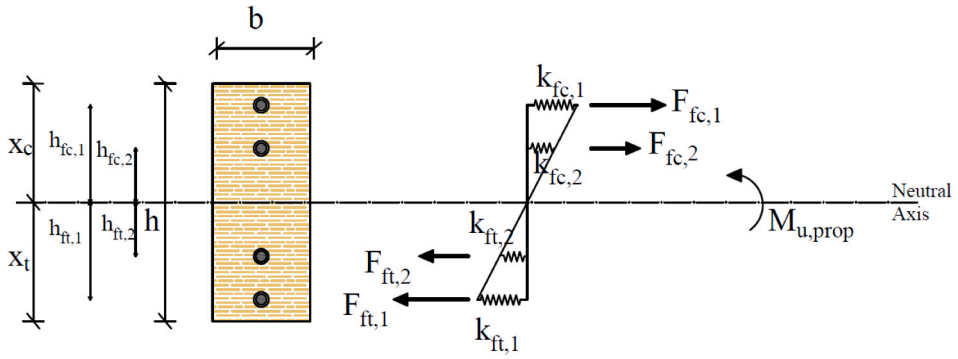

(b) D2

Fig. 15. Model for rotational stiffness prediction.

Table 8
Comparison between experimental and proposed rotational stiffness of the connection.

Specimen	$k_{,Exp}$ (kNm/rad)	$k_{,prop}$ (kNm/rad)	$k_{,prop}/k_{Exp}$
8 - D1–1	1264	1226	0.97
8 - D1–2	1184	1226	1.04
8 - D1–3	883	1226	1.39
8 - D1–4	993	1226	1.23
8 - D2–1	788	785	1.00
8 - D2–2	1184	785	0.66
8 - D2–3	1408	785	0.56
8 - D2–4	796	785	0.99
10 - D1–1	1220	1532	1.26
10 - D1–2	1251	1532	1.22
10 - D1–3	1254	1532	1.22
10 - D1–4	1414	1532	1.08
10 - D2–1	1066	981	0.92
10 - D2–2	1215	981	0.81
10 - D2–3	1202	981	0.82
10 - D2–4	1328	981	0.74
		mean	0.99
		COV	0.24

of a beam subjected to pure bending, the position of the neutral axis defines the limit between the area of the section in tension and the area in compression. The plane cross-section assumption hypothesis which considers that the cross-section remains plane during bending, can allow to geometrically transform a composite section into an equivalent one, multi-plying the width of each material by its corresponding modular ratio [53] and hence has been applied herein.

During testing, the top parts of the connections remained in constant contact indicating the activation of a timber compression zone. However, given the difficulty of accurately predicting the depth of this zone and in order to simplify the proposed model, it is considered that the contribution of the timber in compression is neglected. The tension and compression forces, at the connection, are fully transmitted through the FRP rods only. It is noteworthy that in a preliminary study, the force between the bonded timber members in the compression zone has been taken into account, but this has led to an overestimation (i.e. unsafe) prediction of the strength, compared to the experimental results. Hence, it was decided for the predictions to be on the safe side, thus only considering the forces of the FRP rods in the model. Note that similar approach has been applied in Xu et al. [50]. The model shown in Fig. 14 can be applied to calculate the bending strength of the glued-in rod connections.

Where b and h are the width and depth of the cross-section, x_c and x_t, are depths of the compression and tension zones, respectively, whilst z refers to the distance measured from the centroid of each FRP rod to the corresponding specimen edge. In addition to the cross-section, the strain (ε) distribution and the force diagram (F) are also shown in Fig. 14. The first two characters, namely "f_t" and "f_c", in the subscript of strains, forces and distances, stand for FRP rod in tension and in compression, respectively, whereas the third character denotes the rod number (i.e. rod 1 or 2).

Following the force diagram shown in Fig. 14, the bending moment ($M_{u,prop}$) can be evaluated from Eq. (2)–(3).

$$M_{u,prop} = (F_{ft,1} + F_{ft,2}) * (x_t - z_{ft}) + (F_{fc,1} + F_{fc,2}) * (x_c - z_{fc}) \quad \text{(for D1)} \tag{2}$$

$$M_{u,prop} = F_{ft,1} * (x_t - z_{ft,1}) + F_{ft,2} * (x_t - z_{ft,2}) + F_{fc,1} * (x_c - z_{fc,1}) + F_{fc,2} * (x_c - z_{fc,2}) \quad \text{(for D2)} \tag{3}$$

For the estimation of the bending strength of the connection, it can be considered that the moment capacity is reached when the FRP rod

with the highest tensile stresses (i.e. $F_{ft,1}$), reaches the minimum between its tensile strength and pull out-strength, see Eq. (4). The tensile strength of the rod is equal to its cross-sectional area (A_f) times its yield strength ($f_{f,y}$) which is equal to 920 MPa for the rods studied herein. For the pull-out strength, it is proposed to use the formula (see Eq. (4)) suggested by Yeboah et al. [54], which was based on test data on bonded-in BFRP rod glulam joints.

$$F_{ft,1} = \min \begin{cases} A_f \bullet f_{f,y} \\ \pi \bullet f_v \bullet d_h \bullet l_b \end{cases} \quad (4)$$

Where d_h the hole diameter (herein the hole diameter equals to 14 mm), l_b the embedment length (<=15d_h) and f_v equal to 5.7 MPa.

Upon calculation of $F_{ft,1}$ and considering elastic material properties and pure bending conditions, the moment capacities ($M_{u,prop}$) can be evaluated according to Eq. (2)–(3) and Fig. 14. In Table 7, a comparison between the experimentally achieved bending moments and those evaluated theoretically is presented. Apart from Design D1 specimens with 8 mm rods, it is evident, from Table 7, that the proposed model is capable of predicting with good accuracy the moment capacity of connections with glued-in BFRP rods. The average $M_{u,prop}/M_{u,Exp}$ of groups 8-D2, 10-D1 and 10-D2 is equal to 1.04. This ratio becomes 1.15 when considering also group 8-D1. It is noteworthy that the variation between the specimens of D2, whether it being between the 8 mm or 10 mm groups, is less pronounced when compared to D1 groups. This could be attributed to the fact that Design D1 has two bars close to the edge in comparison to Design D2. The dominant failure modes, as reported before in Section 4.3, were bar pull-out with wood attached and tensile splitting of timber for all specimens. This would indicate that the edge-to-hole clearance (i.e., edge distance) used in D1 designs has caused premature failure that could also be related with existing defects within the lower lamellae, thus resulting in lower experimental bending strength than the predicted by the proposed model. Another contributing factor is the fact that in Design D1 with 8 mm rods the provided glue line is 3 mm (due to the hole size being 14 mm) causing the combined effect of the 8 mm rod with the adhesive to be more stiff placing higher pushing stress on the surrounding timber and accelerating failure. Further testing of Design D1 with different edge-to-hole values are required to confirm this observation.

5.2. Rotational stiffness

In Section 4.1, the experimentally obtained rotational stiffness values of the connections have been reported. In order to estimate these values theoretically, the model shown in Fig. 15 can be applied, where the FRP rods can be represented with springs arranged in parallel [50].

In Fig. 15, $k_{f,i}$ stands for the axial stiffness of each rod. $h_{f,i}$ is the distance between the rod axis and the neutral axis of the connection. In the subscripts, f stands for the FRP, c and t for compression and tension, followed by the rod number. The remaining symbols are as previously defined. The axial stiffness can be calculated from Eq. (5).

$$k_{f,i} = E_{f,i}A_{f,i}/L_{eff,f,i} \quad (5)$$

Where $E_{f,i}$ the Modulus of Elasticity of the FRP equal to 52 GPa herein. $A_{f,i}$, the cross-sectional area of the FRP rod and $L_{eff,f,i}$ the effective embedment length of the rod, respectively.

The force corresponding to each rod ($F_{f,i}$) can be found from Eq. (6)

$$F_{f,i} = k_{f,i} * u_{f,i} \quad (6)$$

Where $u_{f,i}$ the corresponding elongation.

The moment (M) developed by the connection can be estimated via Eq. (7), written as a function of forces and displacements or via Eq. (8), as a function of the rotational stiffness (k_θ) and the connection's angle of rotation (θ)

$$M = \sum F_{f,i} * h_{f,i} = \sum k_{f,i} * u_{f,i} * h_{f,i} \quad (7)$$

$$M = k_\theta * \theta \quad (8)$$

Combining (7) and (8) and considering that the deformation is localised in the connection zone, ($\theta = u_{f,i}/h_{f,i}$) the rotational stiffness of the connection (k_{prop}) can be found from Eq. (9)

$$k_{prop} = k_\theta = \sum (k_{f,i} * h_{f,i}^2) \quad (9)$$

Implementing Eq. (9), a comparison between experimental and proposed values is presented in Table 8. It is noted that Xu et al. [50] have calibrated the value of the effective embedment length (see Eq. (5)) on the basis of numerical and theoretical data on steel-rods glued into timber and found it equal to 0.3 of the actual length. Within this study, close agreement between experimental and theoretical values have been achieved, assuming L_{eff}=0.4 L. For this value, the rotational stiffness has been accurately predicted, with a ratio of $k_{,prop}/k_{Exp}$ equal to0.99, as shown in Table 8.

6. Conclusions

An experimental study, comprising 16 bonded glulam beam specimens fabricated with glued-in BFRP rods, has been presented in this paper. The main findings and observations are summarised below:

(1) Key parameters investigated were the rod diameter (8 mm and 10 mm) and the design configurations (D1, D2: both included two bars on the tension and two on the compression zone, but in D1 the bars were placed in the same horizontal line, whilst in D2 all four bars were in a vertical line).
(2) The global bending stiffness and the rotational stiffness values have been evaluated on the basis of the test data, whereas the load-displacement curves and strain distribution profiles were reported and discussed.
(3) The main failure mode observed was pull-out of bars at tension zone and tensile splitting of timber.
(4) In all cases, the connections comprising 10 mm bars outperformed their counterparts with 8 mm bars, whilst D1 configuration outperformed configuration D2. Best overall performance was achieved by D1 and 10 mm rods.
(5) Two theoretical models were presented. The bending strength was predicted with an average value of $M_{u,prop}/M_{u,Exp}$ equal to 1.15. The rotational stiffness of the connection achieved a ratio of $k_{,prop}/k_{Exp}$ equal to 0.99.
(6) The study has demonstrated that the GiR technique with BFRP rods has the potential to serve as an answer for the rehabilitation of aging existing timber beams.

CRediT authorship contribution statement

Yaser Jemaa: Writing – review & editing, Writing – original draft, Methodology, Investigation, Conceptualization. **David Yeboah:** Writing – review & editing, Writing – original draft, Methodology, Investigation, Conceptualization. **Michaela Gkantou:** Writing – review & editing, Writing – original draft, Methodology, Investigation, Conceptualization.

Declaration of Competing Interest

The authors declare that they have no known competing financial interests or personal relationships that could have appeared to influence the work reported in this paper.

Data Availability

Data will be made available on request.

Acknowledgements

The authors are grateful to the technicians of the Faculty of Engineering and Technology of Liverpool John Moores University for their valuable assistance. In addition, the financial support of Liverpool John Moores University is gratefully acknowledged.

References

[1] L. Gustavsson, R. Sathre, Variability in energy and carbon dioxide balances of wood and concrete building materials, Build. Environ. 41 (7) (2006) 940–951.
[2] J. Custódio, J. Broughton, H. Cruz, Rehabilitation of timber structures: novel test method to assess the durability of bonded-in rod connections, Mater. Struct. 45 (2012) 199–221.
[3] Bowyer, J., Fernholz, K. and Kacprzak, A., 2023. Circularity concepts in wood construction. United Nations and the Food and Agriculture Organization of the United Nations, ECE/TIM/DP/95, Forestry and Timber Section.
[4] Y. Liu, A. Li, J. Cao, D. Yu, J. Zhang, Mechanical properties of timber-concrete connections with steel tube connectors, Sustain. Struct. 2 (2022) 17.
[5] H. Yang, W. Liu, X. Ren, A component method for moment-resistant glulam beam–column connections with glued-in steel rods, Eng. Struct. 115 (2016) 42–54.
[6] J.G. Broughton, A.R. Hutchinson, Adhesive systems for structural connections in timber, Int. J. Adhes. Adhes. 21 (3) (2001) 177–186.
[7] R. Steiger, E. Serrano, M. Stepinac, V. Rajčić, C. O'Neill, D. McPolin, R. Widmann, Strengthening of timber structures with glued-in rods, Constr. Build. Mater. 97 (2015) 90–105.
[8] Buchanan, A., Moss, P. and Wong, N., 2001, March. Ductile moment-resisting connections in glulam beams. In Proceedings of NZSEE conference, Wairakei Resort, Taupo, New Zealand.
[9] Riberholt, H., 1980. Glued steel bolts for glulam.
[10] Harvey, K. and Ansell, M.P., 2003. Improved timber connections using bonded-in GFRP rods (Doctoral dissertation, University of Bath).
[11] E. Toumpanaki, M.H. Ramage, Glued-in CFRP and GFRP rods in block laminated timber subjected to monotonic and cyclic loading, Compos. Struct. 272 (2021) 114201.
[12] H. Zhang, H. Li, A. Dauletbek, R. Lorenzo, I. Corbi, O. Corbi, Research status of glued-in rods connections in wood structures, J. Build. Eng. 65 (2023) 105782.
[13] A.P. Usman, S. Sugiri, Analysis of the strength of timber and glulam timber beams with steel reinforcement, J. Eng. Technol. Sci. 47 (6) (2015) 601–611.
[14] M. Madhoushi, M.P. Ansell, Effect of glue-line thickness on pull-out behavior of glued-in GFRP rods in LVL: Finite element analysis, Polym. Test. 62 (2017) 196–202.
[15] B.F. Donadon, N.T. Mascia, R. Vilela, L.M. Trautwein, Experimental investigation of glued-laminated timber beams with Vectran-FRP reinforcement, Eng. Struct. 202 (2020) 109818.
[16] V. Dhand, G. Mittal, K.Y. Rhee, S.J. Park, D. Hui, A short review on basalt fiber reinforced polymer composites, Compos. Part B: Eng. 73 (2015) 166–180.
[17] A.M. Harte, P. Dietsch, Reinforcement of timber structures: A state-of-the-art reportA.M.HarteP.DietschDürenShakerGermany2015.
[18] M.H. Niaki, A. Fereidoon, M.G. Ahangari, Experimental study on the mechanical and thermal properties of basalt fiber and nanoclay reinforced polymer concrete, Compos. Struct. 191 (2018) 231–238.
[19] M.R. Sanjay, B. Yogesha, Studies on natural/glass fiber reinforced polymer hybrid composites: An evolution, Mater. Today.: Proc. 4 (2) (2017) 2739–2747.
[20] S.S. Vinay, M.R. Sanjay, S. Siengchin, C.V. Venkatesh, Basalt fiber reinforced polymer composites filled with nano fillers: A short review, Mater. Today.: Proc. 52 (2022) 2460–2466.
[21] H. Zhu, P. Faghani, T. Tannert, Experimental investigations on timber joints with single glued-in FRP rods, Constr. Build. Mater. 140 (2017) 167–172.
[22] P. Alam, D. Mamalis, C. Robert, C. Floreani, C.M.Ó. Brádaigh, The fatigue of carbon fibre reinforced plastics-A review, Compos. Part B: Eng. 166 (2019) 555–579.
[23] K. Saad, A. Lengyel, Strengthening timber structural members with CFRP and GFRP: A state-of-the-art review, Polymers 14 (12) (2022) 2381.
[24] C. Wu, Z. Zhang, L. He, L.H. Tam, Experimental study on the static and fatigue performances of GFRP-timber bolted connections, Compos. Struct. 304 (2023) 116435.
[25] S. Kilinçarslan, Y.S. Turker, M. Avcar, Numerical and Experimental evaluation of the mechanical behavior of FRP-strengthened solid and glulam timber beams, J. Eng. Manag. Syst. Eng. 2 (3) (2023) 158–169.
[26] M. Corradi, C.M. Vemury, V. Edmondson, K. Poologanathan, B. Nagaratnam, Local FRP reinforcement of existing timber beams, Compos. Struct. 258 (2021) 113363.
[27] F. Patalas, J. Brol, T.P. Nowak, Numerical analysis, experimental tests and non-linear analytical models in the study of bent timber beams reinforced with FRP strips, Constr. Build. Mater. 399 (2023) 132531.
[28] L.C. Hollaway, J. Teng, G. eds, Strength. Rehabil. Civ. Infrastruct. Using Fibre-Reinf. Polym. (FRP) Compos. Elsevier. (2008).
[29] F. Micelli, V. Scialpi, A. La Tegola, Flexural reinforcement of glulam timber beams and joints with carbon fiber-reinforced polymer rods, J. Compos. Constr. 9 (4) (2005) 337–347.
[30] C. Bengtsson, C.J. Johansson, GIROD-Glued in rods for timber structures, SMT4-CT9 (2002) 7–2199.
[31] K.U. Schober, A.M. Harte, R. Kliger, R. Jockwer, Q. Xu, J.F. Chen, FRP reinforcement of timber structures, Constr. Build. Mater. 97 (2015) 106–118.
[32] Bernasconi, A., 2001. Behaviour of axially loaded glued-in rods–requirements and resistance, especially for spruce timber perpendicular to the grain direction. In Proceedings of the CIB-W18 Meeting Thirty-Four, Venice, Italy, Paper (pp. 34-37).
[33] G.M. Raftery, F. Kelly, Basalt FRP rods for reinforcement and repair of timber, Compos. Part B: Eng. 70 (2015) 9–19.
[34] D. Yeboah, S. Taylor, D. McPolin, Experimental study of interfacial stress distribution of bonded-in BFRP rod glulam joints using fibre optic sensors (FOS) (November), in: Structures, Elsevier, 2016, pp. 53–62 (November).
[35] Baroth, J., Bodé, L., Bressolette, P., Fournely, E. and Racher, P., 2004. Glued-in rod connections in bending: experiment and stochastic finite-element modelling. In World Conference on Timber Engineering (WCTE), Lahti, Finlande.
[36] D.O. Chans, J.E. Cimadevila, E.M. Gutiérrez, Withdrawal strength of threaded steel rods glued with epoxy in wood, Int. J. Adhes. Adhes. 44 (2013) 115–121.
[37] G. Tlustochowicz, E. Serrano, R. Steiger, State-of-the-art review on timber connections with glued-in steel rods, Mater. Struct. 44 (2011) 997–1020.
[38] Gehri, E., 2010, June. High performing jointing technique using glued-in rods. In 11th World Conference on Timber Engineering (Vol. 2010).
[39] V. Gardelle, P. Morlier, Geometric parameters which affect the short-term resistance of an axially loaded glued-in rod, Mater. Struct. 40 (1) (2007) 127–138.
[40] Z. Ling, W. Liu, F. Lam, H. Yang, W. Lu, Bond behavior between softwood glulam and epoxy bonded-in threaded steel rod, J. Mater. Civ. Eng. 28 (3) (2016) 06015011.
[41] M. Madhoushi, M.P. Ansell, Behaviour of timber connections using glued-in GFRP rods under fatigue loading. Part I: In-line beam to beam connections, Compos. Part B: Eng. 39 (2) (2008) 243–248.
[42] M. Madhoushi, M.P. Ansell, Behaviour of timber connections using glued-in GFRP rods under fatigue loading. Part II: Moment-resisting connections, Compos. Part B: Eng. 39 (2) (2008) 249–257.
[43] C. O'Neill, D. McPolin, S.E. Taylor, A.M. Harte, C. O'Ceallaigh, K.S. Sikora, Timber moment connections using glued-in basalt FRP rods, Constr. Build. Mater. 145 (2017) 226–235.
[44] BS EN 17334, 2021. Glued-in rods in glued structural timber products. Testing, requirements and bond shear strength classification. United Kingdom.
[45] Magmatech (2023) RockBar. [online] Available at: < https:// http://magmatech.co.uk/products/rockbar/ [Accessed 20 April 2023].
[46] P. Zhang, Y. Hu, Y. Pang, H. Feng, D. Gao, J. Zhao, S.A. Sheikh, Influence factors analysis of the interfacial bond behavior between GFRP plates, concrete (August), in: Structures, Vol. 26, Elsevier, 2020, pp. 79–91 (August).
[47] Rotafix (2023) Rotafix Manufacturer Structural Adhesive, Cements And Coatings. [online] Available at: < https://rotafix.co.uk/products/timber-engineering/rotafix-engineering-adhesive/> [Accessed 20 April 2023].
[48] D.G. Novidis, S.J. Pantazopoulou, Bond tests of short NSM-FRP and steel bar anchorages, J. Compos. Constr. 12 (3) (2008) 323–333, https://doi.org/10.1061/(ASCE)1090-0268(2008)12:3(323).
[49] D. Yeboah, M. Gkantou, Investigation of flexural behaviour of structural timber beams strengthened with NSM basalt and glass FRP bars (October), in: Structures, Vol. 33, Elsevier., 2021, pp. 390–405 (October).
[50] B.H. Xu, A. Bouchaïr, P. Racher, Analytical study and finite element modelling of timber connections with glued-in rods in bending, Constr. Build. Mater. 34 (2012) 337–345.
[51] H.S. Sousa, J.M. Branco, P.B. Lourenço, January. Glulam mechanical characterization. In Materials Science Forum, Trans. Tech. Publ. Ltd Vol. 730 (2013) 994–999.
[52] O.O. Ekundayo, C. Arum, J.M. Owoyemi, Bending strength evaluation of glulam beams made from selected nigerian wood species, Int. J. Eng. 35 (11) (2022) 2120–2129.
[53] C. Timbolmas, R. Bravo, F.J. Rescalvo, M. Portela, Transformed-section method applied to multispecies glulam timber beams subjected to pure bending, Mech. Adv. Mater. Struct. 29 (27) (2022) 6814–6823.
[54] D. Yeboah, S. Taylor, D. McPolin, R. Gilfillan, Pull-out behaviour of axially loaded Basalt Fibre Reinforced Polymer (BFRP) rods bonded perpendicular to the grain of glulam elements, Construction and Building Materials 38 (2013) 962–969.